Acta Crystallographica Section F
Structural Biology Communications
ISSN 2053-230X

Preliminary crystallographic analysis of the ankyrin-repeat domain of *Arabidopsis thaliana* AKT1: identification of the domain boundaries for protein crystallization

Antonio Chaves-Sanjuán, María José Sánchez-Barrena, Juana María González-Rubio and Armando Albert*

Departamento de Cristalografía y Biología Estructural, Instituto de Química–Física 'Rocasolano', CSIC, Serrano 119, 28006 Madrid, Spain

Correspondence e-mail: xalbert@iqfr.csic.es

Received 16 December 2013
Accepted 6 March 2014

The *Arabidopsis thaliana* K^+ transporter 1 (AKT1) participates in the maintenance of an adequate cell potassium (K^+) concentration. The CBL-interacting protein kinase 23 (CIPK23) activates AKT1 for K^+ uptake under low-K^+ conditions. This process is mediated by the interaction between the cytosolic ankyrin-repeat (AR) domain of AKT1 and the kinase domain of CIPK23. However, the precise boundaries of the AR domain and the residues responsible for the interaction are still unknown. Here, the optimization procedure to obtain an AR domain construct suitable for crystallization and the preliminary crystallographic analysis of the obtained crystals are reported. The crystals belonged to space group $P2_12_12$, with unit-cell parameters a = 34.83, b = 65.89, c = 85.44 Å, and diffracted to 1.98 Å resolution.

1. Introduction

Because of their sessile nature, plants have evolved to adapt to environmental stress situations such as starvation, cold, salt, drought, floods, light *etc.* At the cellular level, the primary stress stimulus is encoded into a fluctuation of the cytosolic calcium (Ca^{2+}) concentration (Allen & Schroeder, 2001). Plant cells have developed a specific family of Ca^{2+} sensors, the calcineurin B-like proteins (CBLs), that provide the molecular machinery to decode this information (Kudla *et al.*, 1999; Luan *et al.*, 2002; Sánchez-Barrena *et al.*, 2005). However, an additional level of regulation is necessary to produce a specific cell response. This is provided by the Ca^{2+}-dependent, CBL-mediated interaction and activation of the CIPK family of protein kinases (Shi *et al.*, 1999). Active CIPKs specifically target a protein substrate to trigger the cell response.

K^+ starvation is one of the most relevant stress situations for plants since K^+ is the most abundant ion in cells and contributes to cell growth and development (Leigh & Jones, 1984). Under low-K^+ conditions, the AKT1 (*Arabidopsis thaliana* K^+ transporter 1) is responsible for K^+ uptake in roots, restoring the proper K^+ concentration inside the cells (Sentenac *et al.*, 1992). It has been shown that the Ca^{2+} sensors CBL1 and CBL9 are involved in AKT1 regulation (Xu *et al.*, 2006). In the presence of Ca^{2+} they interact with CIPK23, which subsequently phosphorylates and activates AKT1 (Xu *et al.*, 2006).

AKT1 is a shaker-like K^+ channel of *Arabidopsis* with a cytoplasmatic region consisting of a cAMP-binding domain and an AR (ankyrin-repeat) domain. The interaction between AKT1 and CIPK23 has been well characterized at the functional and molecular levels and involves the AR domain of AKT1 and the catalytic domain of CIPK23 (Lee *et al.*, 2007). To understand the molecular and structural basis of the regulation of AKT1 by CIPK23, we planned to determine the structure of the AR domain of AKT1. This included construct optimization to remove unstructured regions of the domain, and the purification, crystallization and preliminary crystallographic analysis of the protein.

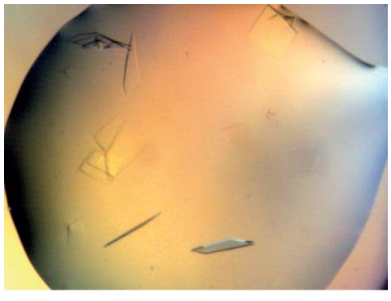

Table 1
Primer information.

Construct	Primer	Sequence
$AKT1_{516–730}$	5′-primer	GGAATTCCATATGGATCTTCCTCTC
	3′-primer	GCGCATGCGGCCGCTCAGAATCTTCCG
$AKT1_{516–715}$	5′-primer	GGAATTCCATATGGATCTTCCTCTC
	3′-primer	CGCGAGCGGCCGCTCACGAAGAACTT
$AKT1_{516–706}$	5′-primer	GGAATTCCATATGGATCTTCCTCTC
	3′-primer	CGCGAGCGGCCGCTCACTCATGTAACTTT

2. Materials and methods

2.1. Gene cloning, protein expression and purification

Three different constructs ($AKT1_{516–730}$, $AKT1_{516–715}$ and $AKT1_{516–706}$) were amplified by PCR using primers that contained *Nde*I and *Not*I restriction sites (Table 1). The amplified product was cloned into pET-28a vector (Novagen) and the final constructs were confirmed by DNA sequence analysis. Recombinant proteins were overexpressed in *Escherichia coli* strain Rosetta 2(DE3)pLysS (Novagen) grown in 2×TY medium. Protein expression was induced with 0.3 m*M* IPTG and the cells were subsquently incubated for 16 h at 16°C. The cells were harvested by centrifugation (20 min, 1300*g*). The bacterial pellet was resuspended and lysed by sonication in a buffer consisting of 20 m*M* HEPES pH 7.0, 150 m*M* NaCl, 0.5 m*M* TCEP. After clarification (45 min, 47 808*g*), the proteins were purified by Ni^{2+}–NTA agarose bead affinity chromatography (Qiagen). The polyhistidine tag located at the N-terminus was cleaved on the column using 10 units of thrombin per milligram of recombinant protein and adding 10 m*M* $CaCl_2$. The cleaved protein was further purified by size-exclusion chromatography, obtaining a unique peak that elutes with an apparent molecular weight corresponding to a monomer (Fig. 1*a*). The eluted proteins were concentrated to 14 mg ml^{-1} using a concentrator with a 10 kDa cutoff membrane (Vivaspin) and frozen at −80°C for subsequent experiments. The sample purity was verified by SDS–PAGE (Fig. 1*b*) and mass spectrometry (MALDI–TOF) (Fig. 1*c*). The observed molecular weight corresponds to that calculated for this construct plus one residue derived from the digestion with the protease.

2.2. Crystallization

Initial crystallization screens were set up as sitting-drop vapour-diffusion experiments. We used an Innovadine crystallization robot and crystallization kits from Qiagen, Hampton Research and Jena Bioscience. Screens were pipetted in 96-well plates with a final drop size of 0.5 µl and a 1:1 mixture of protein and precipitant solutions. Several crystallization conditions produced spherulites, flower-shaped crystals or thin plate-shaped crystals when using the $AKT1_{516–730}$, $AKT1_{516–715}$ or $AKT1_{516–706}$ protein fragments, respectively (Fig. 2). However, after extensive optimization of the crystallization conditions, only those crystals corresponding to the $AKT1_{516–706}$ fragment were suitable for diffraction experiments. The final crystallization condition consisted of 0.1 *M* Tris pH 8.5, 25% PEG 4000, 0.3 *M* $MgCl_2$ and the crystals grew in 3 d at room temperature.

2.3. X-ray analysis

$AKT1_{516–706}$ crystals were cryoprotected with the crystallization solution supplemented with 10%(*v*/*v*) glycerol. They were mounted in a fibre loop and flash-cooled in liquid nitrogen. One data set was collected at the ESRF, Grenoble (Fig. 3 and Table 2). Data were processed with *iMosflm* (Battye *et al.*, 2011) and scaled with *SCALA* (Evans, 2006) from the *CCP*4 package (Winn *et al.*, 2011)

3. Results and discussion

There is a well established relationship between sample homogeneity and success in crystallization. Sample homogeneity can be achieved by the optimization of protein constructs to remove unstructured regions (Derewenda, 2010). This is crucial for multidomain structures in which the domain boundaries are not clearly defined. In particular, the domain structure of AKT1 is poorly defined from a structural point of view. Although AR domains consist of a repetition of a well conserved motif in terms of sequence and structure, the capping repetitions display singularities that challenge the identification of the boundaries.

To figure out the boundaries of the AR domain of AKT1, we performed secondary-structure predictions using the *SCRATCH*

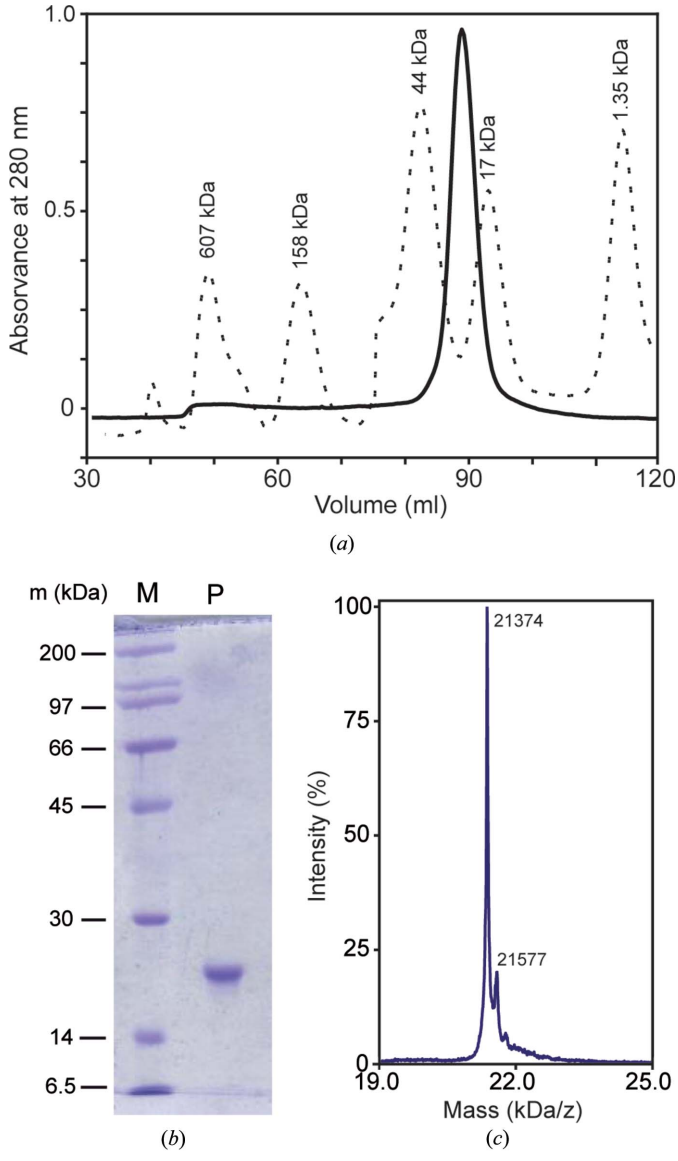

Figure 1
Purification of $AKT1_{516–706}$. (*a*) Size-exclusion chromatography. The solid line shows the elution of $AKT1_{516–706}$ in the presence of 20 m*M* HEPES pH 7.0, 150 m*M* NaCl, 0.5 m*M* TCEP. The dashed line shows elution corresponding to molecular-weight markers (kDa; Gel Filtration Standard, Bio-Rad). (*b*) 12% SDS–PAGE of the final purified sample. Lanes *M* and *P* correspond to molecular-weight marker (labelled in kDa; Low-Range, Bio-Rad) and $AKT1_{516–706}$, respectively. Samples were loaded under reducing conditions. The gel was stained with Coomassie Brilliant Blue (Bio-Rad). (*c*) MALDI–TOF spectrum of the final purified sample.

server (Cheng *et al.*, 2005) and used this information to design different protein constructs. Subsequently, we estimated the crystallizability of those constructs using the *XtalPred* server (Slabinski *et al.*, 2007). The server estimations are based on the statistical analysis of structural genomics data.

The sequence analysis of AKT1 cytosolic region predicted that residues 516–730 include six ankyrin repetitions and an extra α-helix linked by a 15-amino-acid loop. Therefore, as a first approach, we designed a construct containing all these secondary-structure elements ($AKT1_{516–730}$). The overexpressed protein was purified to homogeneity and conditioned for crystallization experiments. The analysis of the commercial crystallization screens showed that $AKT1_{516–730}$ produced spherulites in several conditions (Fig. 2*a*).

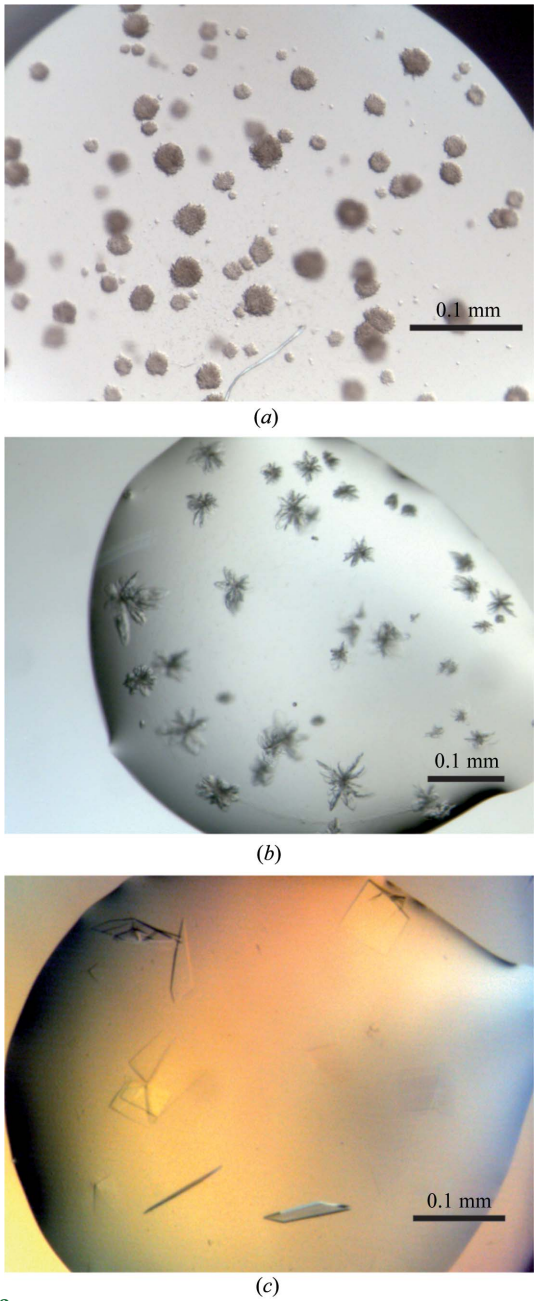

Figure 2
Crystals of the different constructs of AKT1. (*a*) Spherulites obtained with the $AKT1_{516–730}$ construct. (*b*) Flower-shaped crystals grown with the $AKT1_{516–715}$ construct. (*c*) The final diffracting plate-like crystals.

Table 2
Data-collection and processing statistics.

Values in parentheses are for the outer shell.

X-ray source	ID14-1, ESRF
Wavelength (Å)	0.9400
Space group	$P2_12_12$
Unit-cell parameters (Å, °)	a = 34.83, b = 65.89, c = 85.43, $\alpha = \beta = \gamma$ = 90.0
Resolution limits (Å)	52.18–1.98 (2.09–1.98)
$R_{\rm p.i.m.}$† (%)	4.4 (32.5)
$CC_{1/2}$‡	99.6 (74.9)
$\langle I/\sigma(I)\rangle$	7.9 (3.0)
Completeness (%)	98.6 (98.6)
Multiplicity	3.4 (3.5)

† Diederichs & Karplus (1997). ‡ $CC_{1/2}$ is the intra-data-set correlation coefficient calculated from the percentage of correlation between intensities (I_1 and I_2) from random half data sets (Karplus & Diederichs, 2012): $CC_{1/2} = {\rm Corr}(I_1, I_2)$.

However, after extensive optimization of the buffer composition, pH and protein concentration, the crystal quality did not improve and we were not able to perform a successful diffraction experiment. Spherulites are clusters of needle-shaped crystals that grow radially from a single nucleus. These patterns are formed if the crystal growth is hindered in one or two directions owing to conformational or chemical inhomogeneities (Gránásy *et al.*, 2005). Since our sample was chemically homogeneous (Fig. 1*b*), we guessed that protein flexibility was responsible for the formation of spherulites.

The *XtalPred* server estimated enhanced crystallizability for two shortened protein fragments that lacked the predicted C-terminal α-helix included in the original construct. Thus, we cloned, expressed and purified $AKT1_{516–715}$ and $AKT1_{516–706}$ fragments following the previously optimized experimental procedures. The crystallization experiments using the $AKT1_{516–715}$ fragment yielded spherulites and flower-shaped crystals (Fig. 2*b*) but, as with the larger fragment, we were not able to optimize the crystallization condition for diffraction experiments. Instead, the shortened $AKT1_{516–706}$ construct produced plate-like crystals (Fig. 2*c*). These crystals diffracted to 1.98 Å resolution and belonged to space group $P2_12_12$, with unit-cell parameters

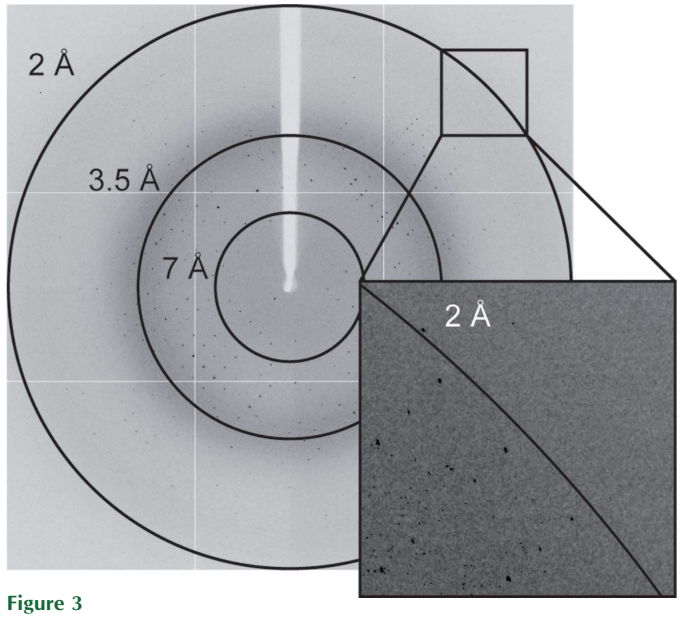

Figure 3
X-ray diffraction pattern of an AR domain crystal from AKT1. The diffraction pattern was obtained using a synchrotron-radiation source. The inset shows a magnification of a sector of the diffraction frame. Numbers show the resolutions (in Å) of the circles.

a = 34.83, b = 65.89, c = 85.44 Å. Diffraction data statistics are shown in Table 2. The high-resolution cutoff was selected considering a value of $\langle I/\sigma(I)\rangle$ greater than 3 to include data to the maximum resolution while maintaining the completeness of the data.

Assuming the presence of one molecule in the asymmetric unit, the Matthews coefficient (V_M) and solvent content were calculated to be 2.31 Å^3 Da^{-1} and 46.7%, respectively (Matthews, 1968). We will address the structure solution by molecular replacement since there are highly conserved AR domain structures with a sequence identity of 54% (PDB entry 1n0q; Mosavi *et al.*, 2002).

We thank María Efigenia Álvarez-Cao for cloning the protein constructs. AA thanks the ESRF (Grenoble) for access to the synchrotron-radiation source. This work was funded by grants from MINECO (BFU2011-25384 and CSD2006-00015 to AA, and BIO2011-28184-C02-02 to MJSB) and Comunidad de Madrid (S2010/BMD-2457 to AA). ACS is supported by a FPI predoctoral fellowship and MJSB by a Ramón y Cajal contract (RYC-2008-03449) from MINECO.

References

Allen, G. J. & Schroeder, J. I. (2001). *Sci. STKE*, **2001**, re13.
Battye, T. G. G., Kontogiannis, L., Johnson, O., Powell, H. R. & Leslie, A. G. W. (2011). *Acta Cryst.* D**67**, 271–281.
Cheng, J., Randall, A. Z., Sweredoski, M. J. & Baldi, P. (2005). *Nucleic Acids Res.* **33**, W72–W76.
Derewenda, Z. S. (2010). *Acta Cryst.* D**66**, 604–615.
Diederichs, K. & Karplus, P. A. (1997). *Nature Struct. Biol.* **4**, 269–275.
Evans, P. (2006). *Acta Cryst.* D**62**, 72–82.
Gránásy, L., Pusztai, T., Tegze, G., Warren, J. A. & Douglas, J. F. (2005). *Phys. Rev. E Stat. Nonlin. Soft Matter Phys.* **72**, 011605.
Karplus, P. A. & Diederichs, K. (2012). *Science*, **336**, 1030–1033.
Kudla, J., Xu, Q., Harter, K., Gruissem, W. & Luan, S. (1999). *Proc. Natl Acad. Sci. USA*, **96**, 4718–4723.
Lee, S. C., Lan, W.-Z., Kim, B.-G., Li, L., Cheong, Y. H., Pandey, G. K., Lu, G., Buchanan, B. B. & Luan, S. (2007). *Proc. Natl Acad. Sci. USA*, **104**, 15959–15964.
Leigh, R. A. & Wyn Jones, R. G. (1984). *New Phytol.* **97**, 1–13.
Luan, S., Kudla, J., Rodriguez-Concepcion, M., Yalovsky, S. & Gruissem, W. (2002). *Plant Cell*, **14**, S389–S400.
Matthews, B. W. (1968). *J. Mol. Biol.* **33**, 491–497.
Mosavi, L. K., Minor, D. L. Jr & Peng, Z. Y. (2002). *Proc. Natl Acad. Sci. USA*, **99**, 16029–16034.
Sánchez-Barrena, M. J., Martínez-Ripoll, M., Zhu, J. K. & Albert, A. (2005). *J. Mol. Biol.* **345**, 1253–1264.
Sentenac, H., Bonneaud, N., Minet, M., Lacroute, F., Salmon, J. M., Gaymard, F. & Grignon, C. (1992). *Science*, **256**, 663–665.
Shi, J., Kim, K.-N., Ritz, O., Albrecht, V., Gupta, R., Harter, K., Luan, S. & Kudla, J. (1999). *Plant Cell*, **11**, 2393–2405.
Slabinski, L., Jaroszewski, L., Rychlewski, L., Wilson, I. A., Lesley, S. A. & Godzik, A. (2007). *Bioinformatics*, **23**, 3403–3405.
Winn, M. D. *et al.* (2011). *Acta Cryst.* D**67**, 235–242.
Xu, J., Li, H.-D., Chen, L.-Q., Wang, Y., Liu, L.-L., He, L. & Wu, W.-H. (2006). *Cell*, **125**, 1347–1360.